Biochimica et Biophysica Acta 1808 (2011) 360–368

Contents lists available at ScienceDirect

Biochimica et Biophysica Acta

journal homepage: www.elsevier.com/locate/bbamem

Solution structure of subunit F (Vma7p) of the eukaryotic V_1V_O ATPase from *Saccharomyces cerevisiae* derived from SAXS and NMR spectroscopy

Sandip Basak [a], Shovanlal Gayen [a], Youg R. Thaker [a], Malathy S.S. Manimekalai [a], Manfred Roessle [b], Cornelia Hunke [a], Gerhard Grüber [a,*]

[a] School of Biological Sciences, Nanyang Technological University, 60 Nanyang Drive, Singapore 637551, Republic of Singapore
[b] European Molecular Biology Laboratory, Hamburg Outstation, EMBL c/o DESY, D-22603 Hamburg, Germany

ARTICLE INFO

Article history:
Received 1 July 2010
Received in revised form 3 September 2010
Accepted 7 September 2010
Available online 15 September 2010

Keywords:
Vacuolar ATPase
V_1V_O ATPase
V_1 ATPase
Vma7p
Subunit F
Small angle X-ray scattering
NMR spectroscopy

ABSTRACT

Vacuolar ATPases use the energy derived from ATP hydrolysis, catalyzed in the A_3B_3 sector of the V_1 ATPase to pump protons via the membrane-embedded V_O sector. The energy coupling between the two sectors occurs via the so-called central stalk, to which subunit F does belong. Here we present the first low resolution structure of recombinant subunit F (Vma7p) of a eukaryotic V-ATPase from *Saccharomyces cerevisiae*, analyzed by small angle X-ray scattering (SAXS). The protein is divided into a 5.5 nm long egg-like shaped region, connected via a 1.5 nm linker to a hook-like segment at one end. Circular dichroism spectroscopy revealed that subunit F comprises of 43% α-helix, 32% β-sheet and a 25% random coil arrangement. To determine the localization of the N- and C-termini in the protein, the C-terminal truncated form of F, $F_{1–94}$ was produced and analyzed by SAXS. Comparison of the $F_{1–94}$ shape with the one of subunit F showed the missing hook-like region in $F_{1–94}$, supported by the decreased D_{max} value of $F_{1–94}$ (7.0 nm), and indicating that the hook-like region consists of the C-terminal residues. The NMR solution structure of the C-terminal peptide, $F_{90–116}$, was solved, displaying an α-helical region between residues 103 and 113. The $F_{90–116}$ solution structure fitted well in the hook-like region of subunit F. Finally, the arrangement of subunit F within the V_1 ATPase is discussed.

1. Introduction

V_1V_O ATPases (V-ATPases) constitute a highly conserved family of proton pumps whose primary function is the establishment of a proton force across membranes by utilization of the free energy from ATP hydrolysis [1,2]. In addition to its major function as a proton pump, the enzyme has been described as an important component of endosomal sensing machinery [3]. As suggested by its bipartite name, the V_1V_O ATPase is composed of a water-soluble V_1 ATPase and an integral membrane subcomplex, V_O. ATP is hydrolyzed on the V_1 headpiece consisting of an A_3:B_3 hexamer, and the energy released during that process is transmitted to the membrane-bound V_O domain, to drive the H^+-translocation [1,2,4–6]. This energy coupling occurs via the so-called "stalk" structure, an assembly of the V_1 and V_O subunits C–H and *a* and *d*, respectively, that forms the functional and structural interface. The integral V_O domain contains five different subunits in a stoichiometry of a_1:d_1:$c_{4–5}$:c'_1:c''_1 [7]. The proposed subunit stoichiometry of V_1 is A_3:B_3:C_1:D_1:E_1:F_1:G_2:H_x [6]. The stalk subunits of the eukaryotic V_1 ATPase solved so far at high resolution are subunit C [8], G [9,10] and H [11] from *Saccharomyces cerevisiae*. Subunit C is formed by an upper head domain, a large globular foot and an elongated neck domain [8]. The elongated subunit G is mainly α-helical [9,10], whereby stalk subunit H is characterized by a large, primarily α-helical N-terminal domain, forming a shallow groove, and a C-terminal domain, connected by a four-residue loop [11].

Together with subunit D, subunit F is shown to form a part of the central stalk, which is directly involved in connecting the cleavage of ATP hydrolysis in the A_3B_3 headpiece with the H^+-pumping process in the V_O part [12]. Subunit F is proposed to undergo structural alterations during catalysis, as it is shown to interact with subunits A, D, and E, dependent on nucleotide occupation in the catalytic sites of the A_3B_3 headpiece [13,14]. In addition, subunit F interacts in the free V_1 ATPase with subunit H, resulting in a drop of ATP hydrolysis [15,16]. Because of the central role of subunit F, insight into its structural features is essential. In this study we have employed a complementary approach of solution X-ray scattering and NMR spectroscopy to analyze the low and high resolution structure of the recombinant subunit F and its C-terminal peptide $F_{90–116}$, respectively. The low resolution solution structure of subunit F provided a unique opportunity to use a subtractive approach of the C-terminal truncated form $F_{1–94}$ to understand the contributions of termini to the overall structure of F and its orientation inside the enzyme complex.

Abbreviations: DSS, 2, 2-dimethyl-2-silapentane-5-sulphonate; NMR, nuclear magnetic resonance; NOE, nuclear Overhauser effect; NOESY, NOE spectroscopy; NMRSD, normalized root mean square deviation; RMSD, root mean square distance

* Corresponding author. Tel.: +65 6316 2989, fax: +65 6791 3856.
E-mail address: ggrueber@ntu.edu.sg (G. Grüber).

0005-2736/$ – see front matter © 2010 Elsevier B.V. All rights reserved.
doi:10.1016/j.bbamem.2010.09.003

2. Materials and methods

2.1. Biochemicals

Pfu DNA Polymerase and Ni^{2+}-NTA-chromatography resin were obtained from Qiagen (Hilden, Germany); restriction enzymes were purchased from MBI Fermentas (St. Leon-Rot, Germany). Chemicals for gel electrophoresis and trypsin used for in-gel digestion were purchased from Serva (Heidelberg, Germany) and Promega (Madison, WI, USA), respectively. All other chemicals were at least of analytical grade and obtained from BIOMOL (Hamburg, Germany), Merck (Darmstadt, Germany), Sigma (Deisenhofen, Germany) or Serva (Heidelberg, Germany).

2.2. Production and purification of subunit F (Vma7p) and F_{1-94} of yeast V_1V_O ATPase

To amplify the *Vma7* coding region, oligonucleotide primers 5′-CTC ACCATGGCTGAGAAACGTACTCTTATAGC-3′ (forward primer) and 5′-GTC CTGAGCTCTTACTCACCGAACAACTTTC-3′ (reverse primer), incorporating *NcoI* and *SacI* restriction sites, respectively, were designed. The *Saccharomyces cerevisiae* genomic DNA was used as the template for the polymerase chain reaction (PCR). The PCR product was ligated into the pET9d-His_3 vector [17], afterwards transformed into *E. coli* cells (strain BL21 (DE3)), which were grown on 30 μg/ml kanamycin-containing Luria–Bertani (LB) agar-plates. To express His_3-F, liquid cultures were shaken in LB medium containing kanamycin (30 μg/ml) for about 20 h at 30 °C until an optical density OD_{600} of 0.6–0.7 was reached. To induce expression of His_3-F, the cultures were supplemented with isopropyl (thio)-β-D-galactoside (IPTG) to a final concentration of 1 mM. Following incubation for another 4 h at 37 °C, the cells were harvested at 8500×*g* for 12 min, 6 °C. Subsequently, they were lysed on ice by sonication for 3×1 min in buffer A (50 mM HEPES, pH 7.0, 300 mM NaCl, 2 mM PMSF and 2 mM Pefabloc^{SC} (BIOMOL)). Precipitated material was separated by centrifugation at 10000×*g* for 35 min. The supernatant was filtered (0.45 μm; Millipore) and passed over a 3 ml Ni^{2+}-NTA resin column to isolate subunit F, according to Grüber et al. [17]. The His-tagged protein was allowed to bind to the matrix for 1.5 h at 4 °C and eluted with an imidazole-gradient (25–400 mM) in buffer A. Fractions containing His_3-subunit F were identified by SDS-PAGE [18], pooled and concentrated as required using Centricon YM-3 (3 kDa molecular mass cut off) spin concentrators (Millipore). Imidazole was removed by gel filtration chromatography using a Superdex 75 HR 10/30 column (GE Healthcare) and a buffer of 50 mM HEPES (pH 7.0), 300 mM NaCl and 5 mM EDTA.

In order to obtain the truncated form of subunit F, F_{1-94}, the primers 5′-CTCACCATGGCTGAGAAACGTACTCTTATAGC-3′ (forward primer) and 5′-GCATGAGCTCTCAAATCTCTAAAATAGCAGGG-3′ (reverse primer) were designed, subsequently cloned and purified as described above. The purity and homogeneity of all protein samples were analyzed by SDS-PAGE [18]. SDS gels were stained with Coomassie Brilliant Blue G250. Protein concentrations were determined by the bicinchoninic acid assay (BCA; Pierce, Rockford, IL., USA). We have also used the corresponding extinction coefficients for protein concentration, resulting in similar values.

2.3. Circular dichroism spectroscopy

Steady state CD spectra were measured in the far UV-light (190–260 nm) using a *Chirascan* spectropolarimeter (Applied Photophysics). Spectra were collected in a 60 μl quartz cell (Hellma) with a path length of 0.1 mm, at 20 °C and a step resolution of 1 nm. The readings were average of 2 s at each wavelength and the recorded ellipticity values were the average of three determinations for each sample. CD spectroscopy of subunit F and the truncated F_{1-94} (2.0 mg/ml) was performed in a buffer of 50 mM HEPES (pH 7.0) and 300 mM NaCl. The spectrum for the buffer was subtracted from the spectrum of the protein. CD values were converted to mean residue ellipticity (Θ) in units of degree $cm^2\,dmol^{-1}$ using the software *Chirascan Version 1.2*, Applied Photophysics. This baseline corrected spectrum was used as input for computer methods to obtain predictions of secondary structure. In order to analyze the CD spectrum the following algorithms were used: Varselec [19], Selcon [20], Contin [21], K2D [22] (all methods as incorporated into the program Dicroprot [23] and Neural Net [24]). The normalized root mean square deviation (NRMSD) was calculated according to Whitmore and Wallace [25].

2.4. X-ray scattering experiments and data analysis of subunit F and F_{1-94}

Small angle X-ray scattering (SAXS) data for subunit F and F_{1-94} were collected by following standard procedures on the X33 SAXS camera [26,27] of the EMBL Hamburg located on a bending magnet (sector D) on the storage ring DORIS III of the Deutsches Elektronen Synchrotron (DESY). A photon counting Pilatus 1 M pixel detector (67×420 mm^2) was used at a sample – detector distance of 2.4 m covering the range of momentum transfer $0.1<s<4.5\ nm^{-1}$ ($s=4p\ \sin(q)/l$, where q is the scattering angle and $l=0.15$ nm is the X-ray wavelength). The s-axis was calibrated by the scattering pattern of Silver-behenate salt (d-spacing 5.84 nm). The scattering from the buffer alone was measured before and after each sample measurement and the average of the scattering before and after each sample is used for background subtraction. A range of protein concentrations (2.5 to 7.4 mg/ml) was measured for both yeast subunit F and F_{1-94} to assess and remove any concentration-dependent inter-particle effects. Both proteins have been measured in a buffer, composed of 50 mM HEPES (pH 7.0), 300 mM NaCl and 1 mM DTT. The protein as well as the buffer samples have been injected automatically using the sample-changing robot for solution scattering experiments at the SAXS station X33 [28]. All the data processing steps were performed automatically using the program package PRIMUS [29]. The forward scattering $I(0)$ and the radius of gyration R_g were evaluated using the Guinier approximation [30] assuming that for spherical particles at very small angles ($s<1.3/R_g$) the intensity is represented by $I(s)=I(0)\ exp(-(sR_g)^2/3)$. These parameters were also computed from the entire scattering patterns using the indirect transform package GNOM [31], which also provide the distance distribution function $p(r)$ of the particle as defined:

$$p(r) = 2\pi\int I(s)sr\sin(sr)ds.$$

The molecular mass of both proteins were calculated by comparison with the forward scattering from the reference solution of bovine serum albumin (BSA). From this procedure a relative calibration factor for the molecular mass (MM) can be calculated using the known molecular mass of BSA (66.4 kDa) and the concentration of the reference solution by applying

$$MM_p = I(0)_p / c_p \times \frac{MM_{st}}{I(0)_{st} / c_{st}}$$

where $I(0)_p$, $I(0)_{st}$ are the scattering intensities at zero angle of the studied and the BSA standard protein, respectively, MM_p, MM_{st} are the corresponding molecular masses and c_p, c_{st} are the concentrations. Errors have been calculated from the upper and the lower I(0) error limit estimated by the Guinier approximation.

Low resolution models of the subunit F and F_{1-94} were built by the program DAMMIN [32,33], which represents the protein as an assembly of dummy atoms inside a search volume defined by a sphere of the diameter D_{max}. Starting from a random model, DAMMIN employs simulated annealing to build a scattering equivalent model fitting the experimental data $I_{exp}(s)$ to minimize discrepancy:

$$\chi^2 = \frac{1}{N-1}\sum_j \left[\frac{I_{exp}(s_j) - cI_{calc}(s_j)}{\sigma(s_j)}\right]^2$$

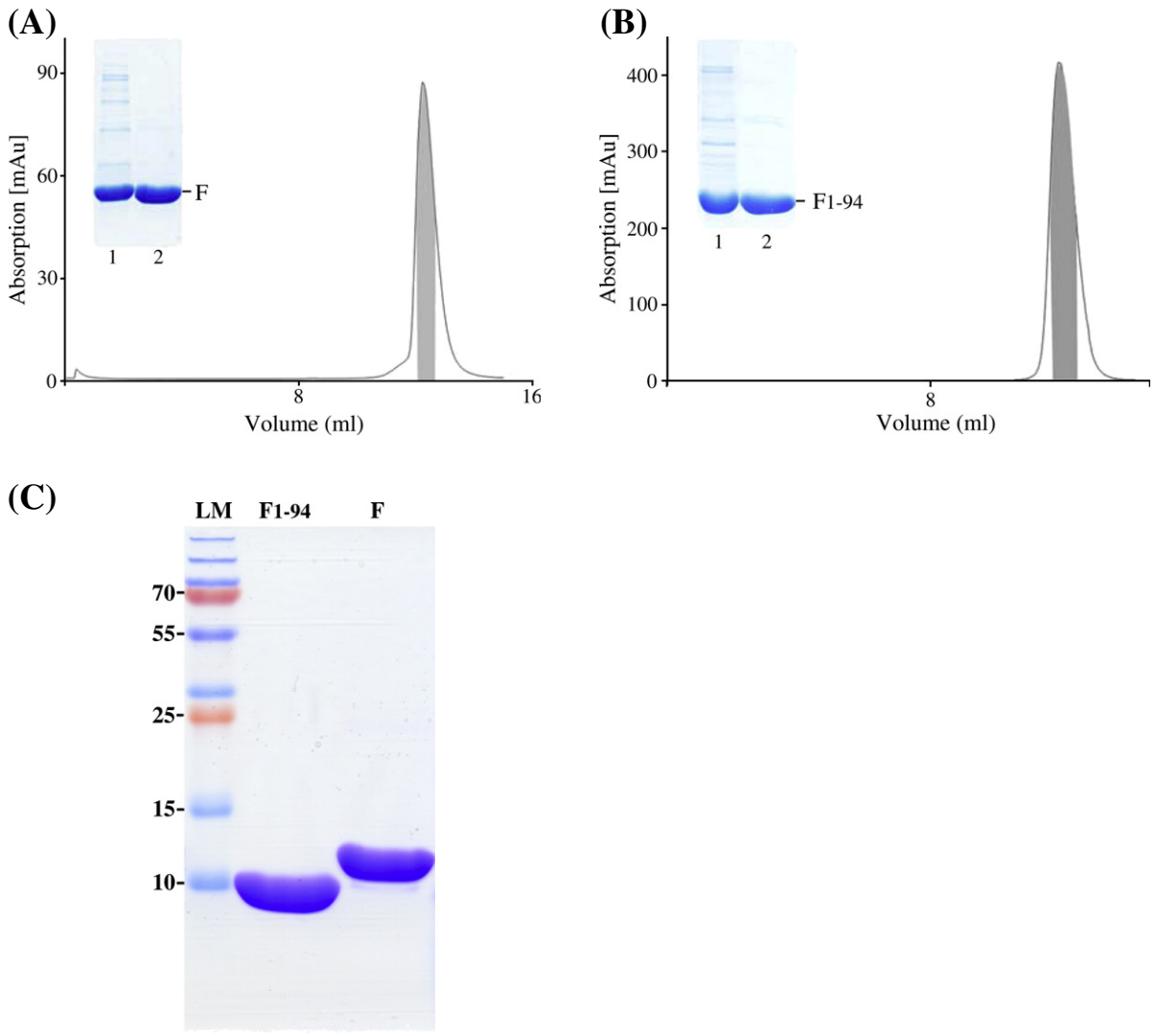

Fig. 1. Purification of *S. cerevisiae* subunit F (Vma7p) (A) and the C-terminal truncated form of subunit F, F_{1-94} (B). Following purification on Ni^{2+}-NTA resin, the proteins were applied onto a Superdex 75 column using buffer (50 mM HEPES, pH 7.0, 300 mM NaCl, 5 mM EDTA) at a flow rate of 0.5 ml/min. Insert in figures showing SDS gels after purification on Ni^{2+}-NTA resin (*lane 1*), indicated fraction from elution peaks after Superdex 75 (*lane 2*) of subunit F (A) and F_{1-94} (B), respectively. (C) SDS-PAGE of purified subunit F and F_{1-94} with protein marker in lane 1.

where N is the number of experimental points, c a scaling factor and $I_{calc}(s_j)$ and $\sigma(s_j)$ are the calculated intensity and the experimental error at the momentum transfer s_j, respectively. *Ab initio* shape models for subunit F and F_{1-94}, respectively were obtained by superposition of ten independent DAMMIN reconstructions for each subunit by using the program package DAMAVER [34].

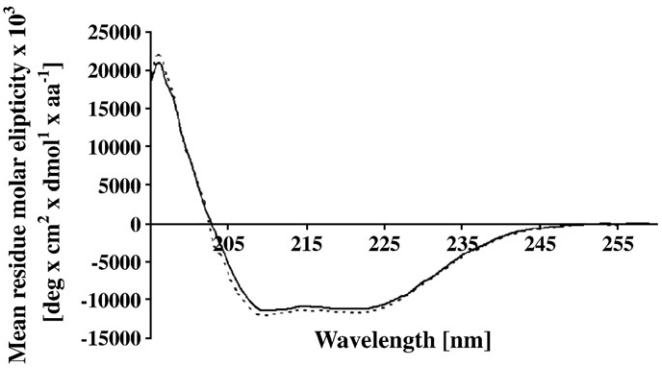

Fig. 2. Far UV-CD spectrum of subunit F (- -) and the truncated F_{1-94} (—).

2.5. Peptide synthesis

The C-terminal peptide F_{90-116} of subunit F from *S. cerevisiae* was synthesized and purified by reversed phase high pressure liquid chromatography at the Division of Chemical Biology and Biotechnology, School of Biological Sciences, Nanyang Technological University, Singapore. The purity and identity of the peptides were confirmed by HPLC and electrospray ionization mass spectrometry (ESI-MS).

2.6. NMR spectroscopy of F_{90-116} from S. cerevisiae

All NMR experiments were performed on a Bruker DRX 600 MHz spectrometer equipped with a cryoprobe. For structure determination appropriate amount of peptide F_{90-116} was dissolved in 25 mM phosphate buffer, pH 6.5. TOCSY and NOESY spectra of the peptide were recorded with mixing times of 80 and 300 ms respectively at a temperature of 25 °C. TopSpin (Bruker Biospin) and Sparky suite [35] of programs were used for spectra processing, visualization and peak

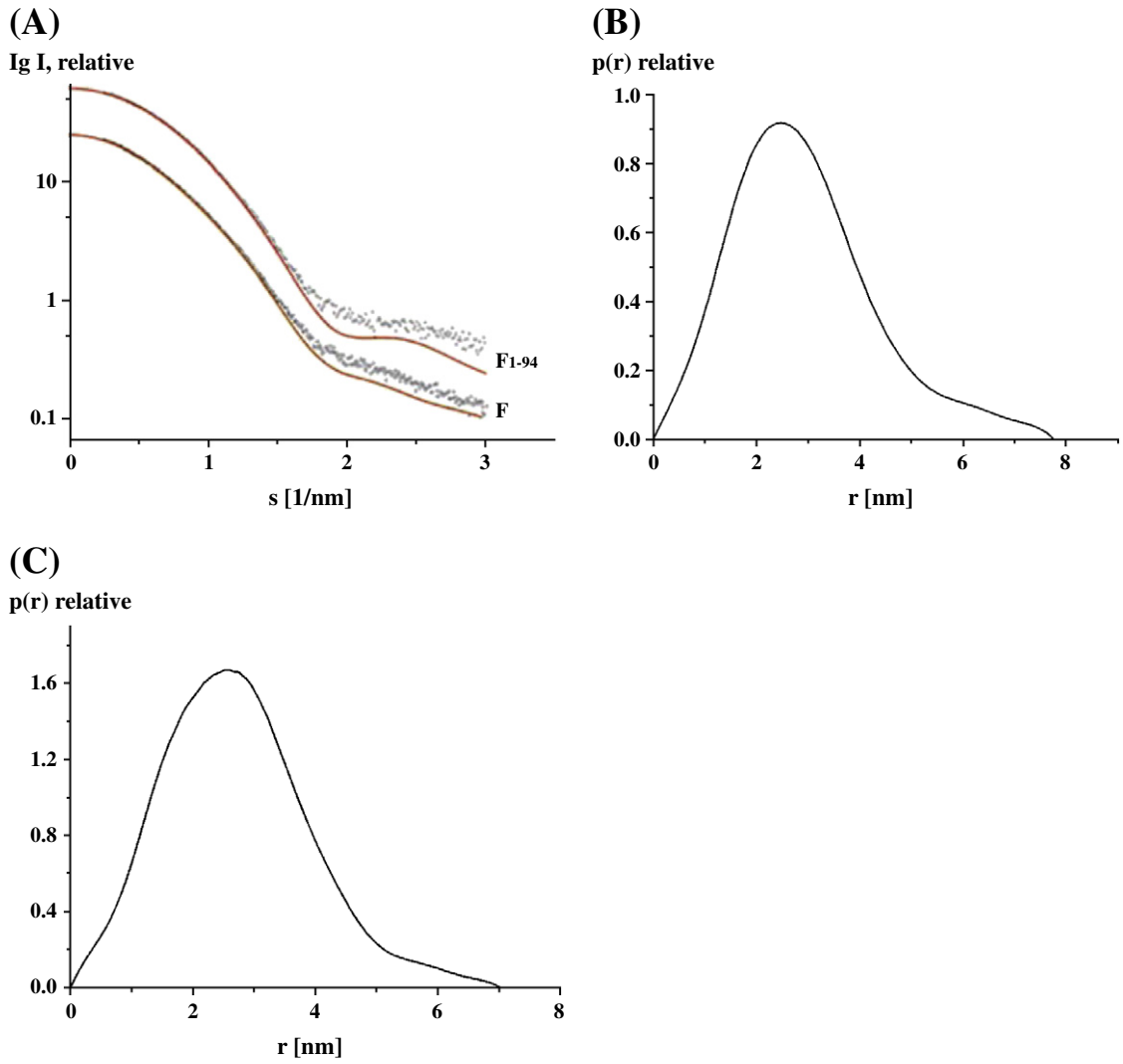

Fig. 3. (A) Experimental scattering curves (●) and the fitting curves (—; *green*: experimental, *red*: calculated from *ab initio* model) of subunit F and F_{1-94}. (B, C) distance distribution functions of subunit F and F_{1-94}, respectively. The curves of subunit F and F_{1-94} are displaced down by a logarithmic unit for clarity.

picking. Standard procedures based on spin-system identification and sequential assignment was adopted to identify the resonances [36]. Inter proton distance were obtained from the NOESY spectra. NOESY peaks were categorized as strong, medium and weak based on the signal intensity and were translated into distance constraints as 3.0 Å, 4.0 Å and 5.0 Å, respectively. Dihedral angle restraints as derived from TALOS [37] were employed to generate the three-dimensional structure of the peptide in the CYANA 2.1 package [38]. In total 100 structures were calculated and an ensemble of 10 structures with lowest total energy was chosen for structural analysis.

3. Results

3.1. Production, purification and secondary structure content of subunit F

Induction of His-tagged protein production under the conditions specified resulted in a soluble 14 kDa protein, representing subunit F of the *S. cerevisiae* V_1V_O ATPase. Ni^{2+}-NTA affinity chromatography has been used in the first purification step. Subunit F was eluted by an imidazole-gradient (25–400 mM) in buffer consisting of 50 mM HEPES (pH 7.0) and 300 mM NaCl. Protein eluting at 75 to 200 mM imidazole was collected and subsequently applied to a Superdex 75 column (Fig. 1A, *lane 1*) in order to isolate a pure and monodispersed protein. Analysis of the isolated protein by SDS-PAGE revealed the high purity of the protein (Fig. 1C). Matrix-assisted laser desorption/ionization (MALDI) mass spectrometry showed that the dehydrated protein of 118 amino acid residues has a mass of 13,685.82 Da, confirming the sequence-based predicted mass.

The secondary structure of recombinant subunit F was determined from circular dichroism spectra, measured between 190 and 260 nm (Fig. 2). The maximum at 192 nm and the minima at 208 and 222 nm indicate the presence of α-helical structures in the protein. The average secondary structure content was 43% α-helix, 32% β-sheet and 25% random coil. This result is consistent with secondary structure predictions based on subunit F amino-acid sequence, revealing an α-helical-, β-sheet- and random coil content of 45% α-helix, 30% β-sheet and 25% random coil, respectively. The normalized root mean square deviation (NRMSD) of the experimental and calculated spectra was 0.06. The molar ellipticity values at 208 nm and at 222 nm are in a ratio of 0.98.

3.2. Low resolution structure of V-ATPase subunit F in solution

The high purity allowed small angle X-ray scattering experiments to be performed, with the aim to determine the first low resolution structure of

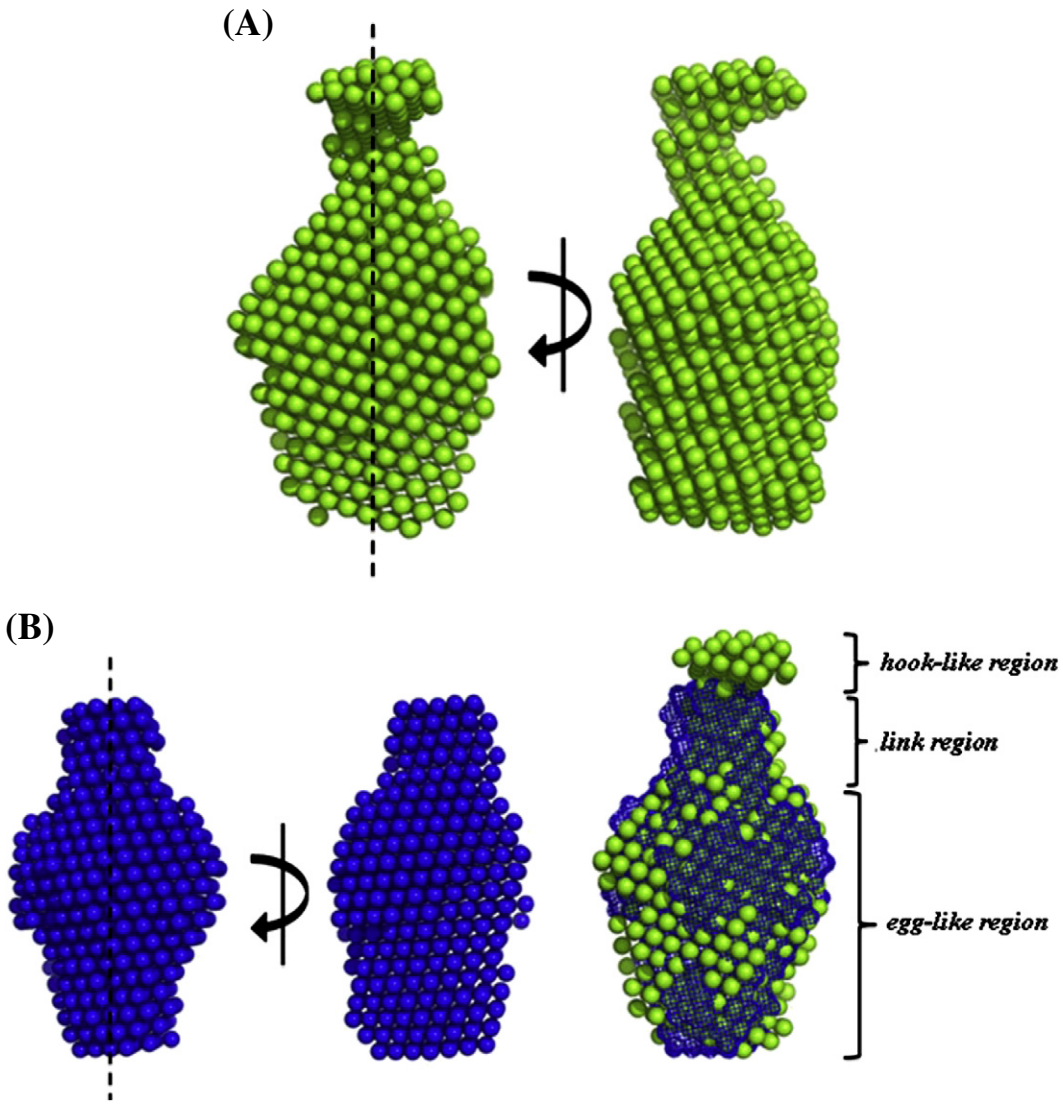

Fig. 4. Low resolution structures of subunit F in green (A), truncated F_{1-94} in blue and their superimposed model (B).

eukaryotic V-ATPase subunit F in solution. SAXS patterns from solutions of the protein were recorded as described in Materials and methods to yield the final composite scattering curve in Fig. 3A, indicating that the protein is monodispersed in solution. Inspection of the Guinier plots of subunit F at low angles indicated good data quality and no protein aggregation. The radius of gyration R_g of subunit F is 2.28 ± 0.3 nm and the maximum dimension D_{max} of the protein is 7.7 ± 0.3 nm (Fig. 3B). Comparison of the forward scattering with the values obtained from a reference solution of bovine serum albumin, (BSA; 66.4 ± 2 kDa) yields a molecular mass of 14 ± 2 kDa, in agreement with the results of the gel filtration chromatography and indicating that subunit F is monomeric at the concentrations used. Qualitative analysis of the distance distribution function suggests that subunit F consists of a major portion, yielding a principal maximum in the $p(r)$ around 2.8 nm (Fig. 3B), whereas the separated protuberance domain giving rise to a shoulder from 5.8 nm to 7.7 nm.

The gross structure of subunit F was restored *ab initio* from the scattering patterns in Fig. 3A. The obtained shape for the protein yields a good fit to the experimental data in the entire scattering range. The corresponding fit, shown in Fig. 3A, has a discrepancies of $\chi = 1.349$. All ten independent reconstructions yielded a reproducible shape and have been averaged (Fig. 4A). The protein appears as a two domain molecule with a large egg-like shape, connected via a 1.5 nm long stalk to a small hook-like region at the end. The major domain has dimensions of about 5.5×3.3 nm, whereby the hook-like segment is about 0.89 nm in length and 2.23 nm width.

3.3. Production and secondary structure of the truncated form of subunit F, F_{1-94}

The N- and C-terminus of subunit F have been predicted to be globular and extended, respectively [7]. In order to find out whether the C-terminus of subunit F may form the hook-like segment, the C-terminal truncated form of subunit F, F_{1-94} was constructed. The expressed polypeptide was purified by metal chelate affinity chromatography (Fig. 1B) and gel filtration (Superdex 75 column) (Fig. 1B). Analysis of the isolated protein by MALDI mass spectrometry revealed masses of 11,155.94 Da. The proper folding of F_{1-94} was confirmed by CD spectroscopy, resulting in a secondary structure composition of 40% α-helix, 32% β-sheet and 28% random coil (Fig. 2) and an NRMSD of 0.05. These data are in line with values derived from secondary structure predictions (39% α-helix, 31% β-sheet and 30% random coil).

3.4. Shape and domain structure of F_{1-94}

F_{1-94} was further investigated by SAXS to determine whether or not the truncation on the C-terminus was accompanied by changes in the

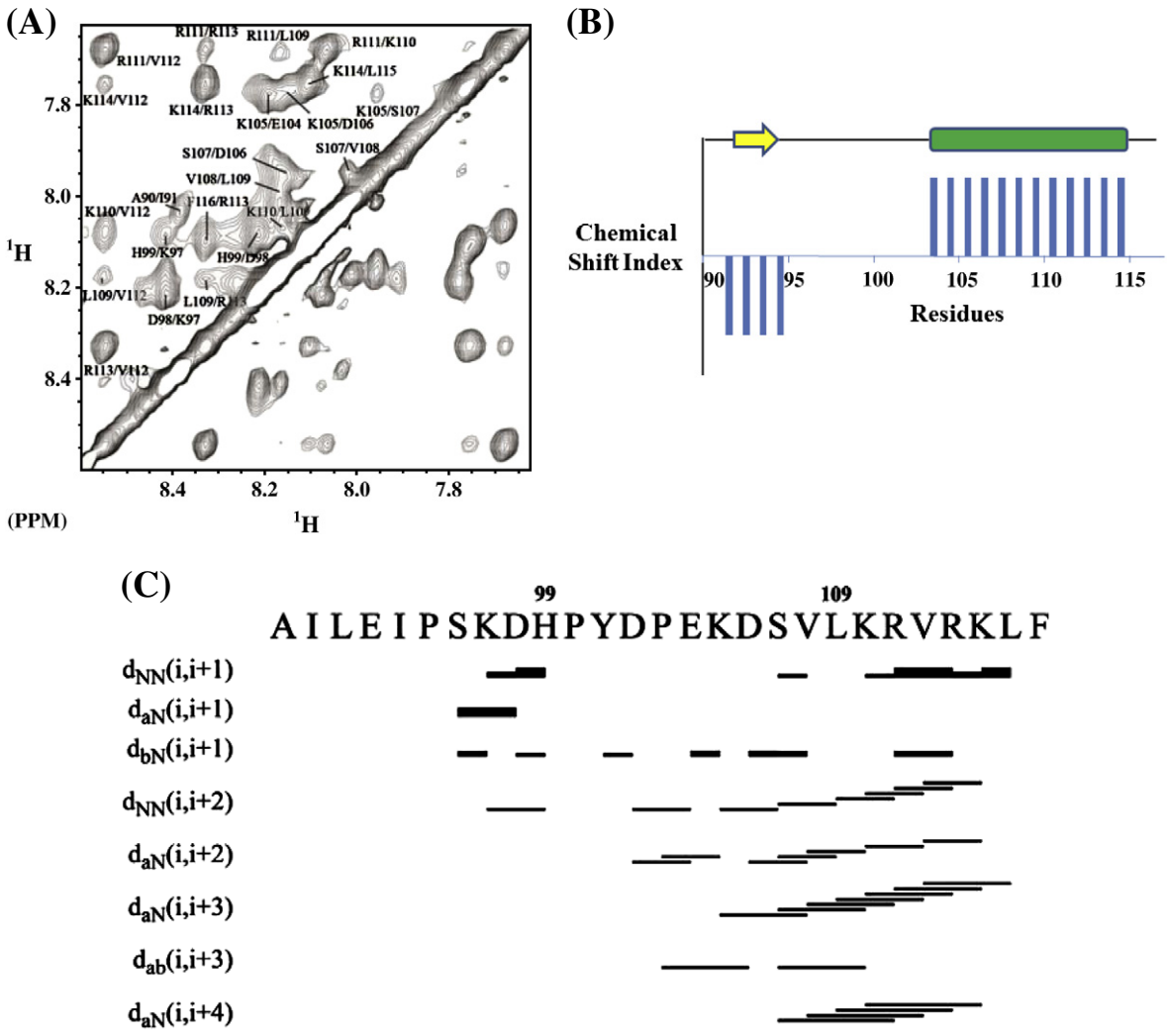

Fig. 5. (A) Assignment of cross peaks in the NOESY spectrum of F_{90-116} in the HN–HN region of the spectrum. Peak picking was done in Sparky 3.1 software and cross peaks were identified based on TOCSY and NOESY spectrum. (B) Secondary structure prediction using Hα chemical shifts of F_{90-116} by PREDITOR software [54]. (C) The NOESY connectivity plot of peptide F_{90-116}.

quaternary structure of the protein. The experimental solution scattering curve of the F_{1-94} protein is presented in Fig. 3A. The obtained shape for F_{1-94} yields a good fit to the experimental data in the entire scattering range with a discrepancies of $\chi^2 = 1.175$ (Fig. 3A). Compared with the SAXS-data of subunit F the radius of gyration of the truncated protein dropped slightly 0.19 ± 0.02 nm, whereas the maximum dimension of the truncated protein decreased significantly ($D_{max} = 7.0 \pm 0.3$ nm). Comparison of the forward scattering with the values obtained for BSA yields a molecular mass of 12 ± 2 kDa.

The low resolution shape of the F_{1-94} form determined *ab initio* is shown in Fig. 4B. Like the entire F subunit, the F_{1-94} form has an egg-like shape. However, comparison with the shape of entire subunit F indicates that the truncation of 24 amino acids at the C-terminus of subunit F results in a loosening of the hook-like region of the molecule (Fig. 4B), which is reflected by the decreased D_{max} value (Fig. 3C). An intriguing observation is that the dimensions and shape of the larger domain of both molecules does not alter implying that the C-terminus of subunit F is located in the upper, hook-like domain.

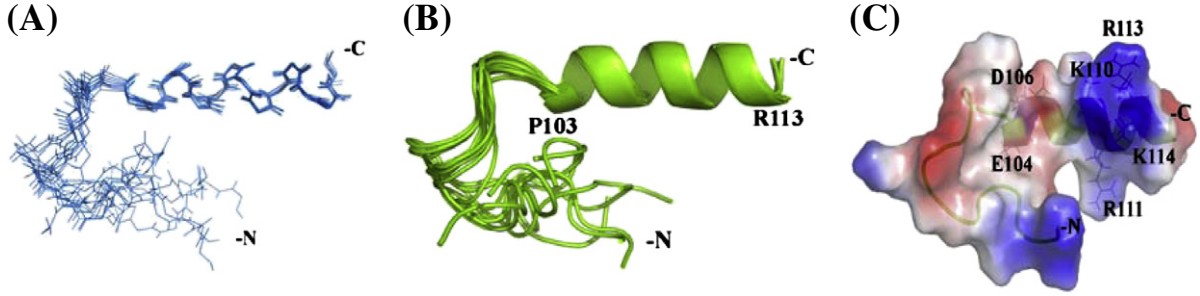

Fig. 6. Superimposition of the 10 lowest energy NMR structures of F_{90-116} in line- (A) and cartoon representation (B). (C) The molecular surface electrostatic potential of peptide F_{90-116} generated by Pymol [55], where the positive potentials are drawn in blue and negative in red.

Table 1
Structural statistics for F_{90-116}.

Total number of residues	27
Total number of NMR restraints	410
Intraresidual (|i−j|=0)	51
Short range (|i−j|≤1)	69
Medium range (2≤|i–j|≤5)	94
Long range (|i−j|>5)	2
Dihedral angle constraints	30
Ramachandran plot statistics (%)	
Residues in most favoured regions	58.2
Residues in additionally allowed regions	30.5
Residues in generously allowed regions	11.4
Residues in disallowed region	0
Structural precision for well ordered region	
RMSD backbone (15–27)	0.303 Å
RMSD heavy atoms	1.46 Å

3.5. Solution structure of F_{90-116}

To get a deeper insight into the solution behavior of the hook-like region, the NMR solution structure of the 27-mer region $_{90}$AILEIPSKDH PYDPEKDSVL KRVRKLF$_{116}$, called F_{90-116}, has been determined. Using standard procedures for sequential assignment based on homonuclear TOCSY and NOESY experiments [36], all the residues of the peptide were assigned (Fig. 5A). Secondary structure prediction was done by using the HA chemical shifts, which shows the presence of α-helical structure at the C-terminus of the peptide between residues P103–R113 (Fig. 5B). Identified cross peaks in HN–HN region are shown in Fig. 5B. HN–HN, Hα–HN(i, i+3), Hα–HN(i, i+4), and Hα–Hβ (i, i+3) connectivity were plotted from the assigned NOESY spectrum (Fig. 5C) also supports α-helical formation in the C-terminus. Two long-range NOEs are observed between residues Y12 HD1 to D17 HB2 and Y12 HE1 to D17 HB2. These NOEs as well as some medium range NOEs, especially NOEs associated with the three proline residues P6, P11 and P14 (P6 HD2 to H10 H, P6 HD2 to H10 HB2, P6 HD2 to H10 HD1, K8 H to H10 H, S7 HA to H10 HD1, Y12 HE1 to P14 HA, Y12 HD1 to P14 HA, D13 HA to E15 H, D13 H to E15 H, H10 HB2 to Y12 H, H10 HB2 to Y12 HE1, P11 HD2 to D13 H, Y12 HD1 to P14 HB2, Y12 HD1 to P14 HD2, Y12 HE1 to P14 HB2, Y12 HE1 to P14 HG2, Y12 HE1 to P14 HD2) stabilize the bending locally in the structure. Out of 100 structures generated, the 10 lowest energy structures were taken for further analysis. In total an ensemble of 10 calculated structures resulted in an overall mean root square deviation (RMSD) of 0.303 Å for the backbone atoms and 1.46 Å for the heavy atoms (Figs. 6A and B). All these structures have energies lower than −100 kcal/mol, no NOE violations greater than 0.3 Å and no dihedral violations greater than 5°. The summary of the statistics for 10 structures are shown in Table 1. The calculated structure has a total length of 27.30 Å displaying an α-helical region between residues 103–113 (14.9 Å) and a flexible N- and C-terminal region, formed by the amino acids 90–102 as well as residues 114–116, respectively (Fig. 6B). Molecular surface electrostatic potential of the peptide is shown in Fig. 6C. The charged distribution of the helix shows mainly a positive charged surface formed by residues K110, R111, R113 and K114.

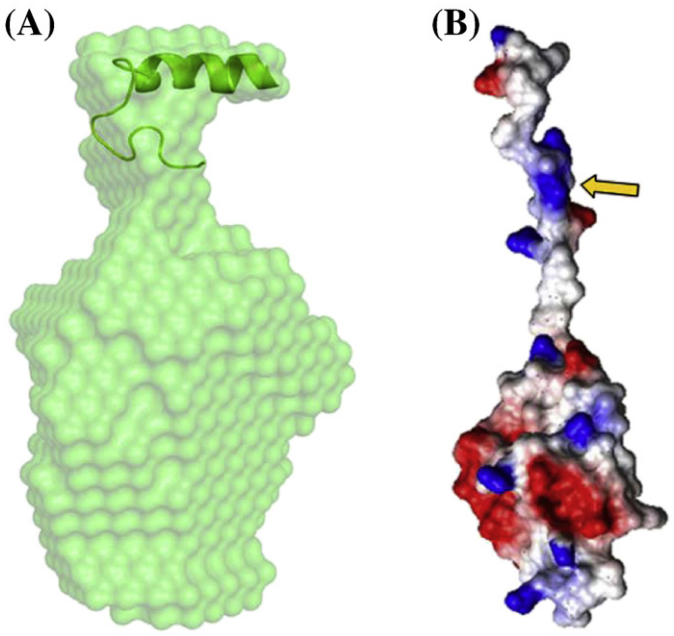

Fig. 7. (*A*) Superimposition of solution structure of F_{90-116} onto SAXS structure of subunit F. (*B*) Molecular surface with the electrostatic potential of the subunit F_{Mm} of the methanogenic A_1Ao ATP synthase [46]. Red and blue areas are negatively and positively charged areas, respectively, calculated with the program Pymol [55]. The arrow indicates the positively charged residues in the C-terminus of F_{Mm}, forming a crosslink with the C-terminus of subunit B [41].

4. Discussion

Small angle scattering of X-rays is an established method providing three-dimensional low resolution structures in solution and is highly complementary to the higher resolution methods of NMR spectroscopy and X-ray crystallography [39] as demonstrated for the solution structures of the *E. coli* F_1 ATPase [40], the chitin binding protein, CHB1 [33], the F subunit of the A_1A_O ATP synthase [41] or subunit C of the *S. cerevisiae* V-ATPase [42], whose structural features were confirmed by X-ray crystallography [8,43,44] or NMR spectroscopy [45,46]. The presented comparison of the low resolution solution structure of F, composed of a major domain, which is connected by a linker segment to the hook-like region (Fig. 4B), with the shape of F_{1-94} unequivocally demonstrates that the missing hook-like segment in F_{1-94} is formed by the C-terminal peptide $_{95}$PSKDHP YDPEKDSVLK RVRKLFGE$_{118}$. The NMR peptide structure of yeast F_{90-116} enabled us to superimpose the peptide and the solution shape of yeast subunit F with the program SUBCOMP [34]. As revealed in Fig. 7A the NMR structure of F_{90-116} fitted well in the hook-like region of subunit F with an r.m.s. deviation of 1.24 Å, supporting that the missing C-terminus of F_{1-94} forms the hook-like segment and, that the major domain of subunit F consists of the N-terminal amino acids sequence.

Although the solution structure of subunit F of the *S. cerevisiae* V-ATPase (F_{Sc}) shows sequence identity of only 15% to subunit F of the A_1A_O ATP synthase from *Methanococcus mazei* Gö1 (F_{Mm}), a well defined N- and C-terminal region was described for the SAXS- (41) and NMR derived (46) solution structure of F_{Mm} (Fig. 7B). In addition, similar structural features are also revealed from the crystallographic structure of the A_1A_O ATP synthase subunit F from *Thermus thermophilus* (F_{Tt}) [47]. These high resolution structures show an alternating arrangement of β-sheet and α-helix, a secondary structural pattern also observed by the mixed content for F_{Sc} as determined by CD spectroscopy (Fig. 2). Also comparable with subunit F of the A_1A_O ATP synthase and F_{Sc} of the eukaryotic V_1V_O ATPase is the α-helical peptide at the very C-terminus [48]. By contrast, both the solution structure of the A_1A_O ATP synthase subunit F_{Mm} derived from SAXS [41] and NMR [46] show that the dimensions of the N-terminal globular domain are smaller when compared to the shape of the one in the V-ATPase subunit F, and that the very C-terminal residues 79–101 form an extended stretch (Fig. 7B). This C-terminal extension makes the 101 amino acid subunit F_{Mm} with a D_{max} of 7.8 nm [41] as long as the subunit F_{Sc} with a total length of 7.7 nm and made up of 118 amino acid residues. As the C-terminal helix of F_{Mm} is directly involved in connecting the H^+-pumping process with catalytic events in the A_3B_3-hexamer of the A_1A_O ATP synthase [41,46,48], the diversity of a hook-like and extended C-terminus of the solution structure of F_{Sc} and F_{Mm}, respectively, may cause a different mechanism of coupling in the V-ATPase and A_1A_O ATP synthase.

Also determined from solution X-ray scattering data was the hydrated V_1 ATPase from *Manduca sexta* [40], showing that the central stalk is rather elongated with 11 nm in length and longer than the one of the subunit C depleted $V_1(-C)$ complex of about 7 nm, determined from the 3D reconstruction of this complex [12]. This difference is due to the missing C subunit in the $V_1(-C)$ complex, as shown by electron-microscopy of a reconstituted *M. sexta* $V_1(+C)$ complex [49]. The maximum dimension of 7.7 nm of F_{Sc} would nicely traverse the length of the central stalk and enable this subunit to be in close neighbourhood to the catalytic A_3B_3-headpiece via its C-terminal helix and with its major domain linked to subunit C, which has no counterpart in A_1A_O ATP synthases [6]. The diversity in stalk composition may therefore reflect the need of different structural features of the coupling elements as described above for the hook-like region of V-ATPase subunit F.

V-ATPases exist in a dynamic equilibrium between fully assembled complexes and reversibly disassembled V_1 and V_O subcomplexes [2]. Since the assembled V_1V_O ATPase and the dissociated V_1 complex as well as the coupling process are of physiological relevance, the topology of these stalk subunits are of great interest. It is known, that the stalk subunits undergo rearrangements when the V_1 ATPase reassembles with the V_O domain to form the entire V_1V_O complex. Such rearrangements are shown in experiments, in which H–E, H–F crosslinks are observed in the V_1 domain and C–E crosslink in the V_1V_O ATPase [16,50]. In addition, the arrangement of the stalk subunits, which are involved in the coupling process of ATP hydrolysis and proton pumping, is nucleotide dependent. A strong D–F formation in V_1 ATPase is observed in the presence of CaADP [14], reflecting the close proximity of both subunits in the central stalk. As shown by $CuCl_2$-induced disulfide formation, binding of CaATP to the V_1 part results in the zero-length crosslink products E–F and E–G, as demonstrated for the *M. sexta* V_1 ATPase [13]. By comparison, no disulfide bond could be observed in the absence of nucleotides [13]. Recently, residues involved in the interaction of subunit E and G of the V-ATPase have been determined by NMR titration experiments [9]. Since two cysteine residues must have their α-carbon atoms within 0.4–0.9 nm of each other for a disulfide bond to be formed [51], the data reveal a close proximity of subunit E and F when MgATP is bound to the *M. sexta* V_1 ATPase. Subunit E and F of *M. sexta* V-ATPase has one [52] and two N-terminal cysteine residues (C21, C55 [53]), respectively. Since the presented low resolution structures of F and $F_{1–94}$ reveal, that the N-terminal amino acids form the major domain of subunit F of the V-ATPase (Fig. 4A), we propose that a nucleotide-dependent rearrangement of the N-terminal domain of subunit F with subunit E are involved in coupling events of the V_1 ATPase complex.

In summary the data presented demonstrate that subunit F of the yeast V-ATPase in solution exists as a well defined two domain protein, with an egg-like N-terminal region and a C-terminal hook-like feature, including an α-helical stretch. Together with the NMR structure of the C-terminal peptide $F_{90–116}$, this first low resolution structure of a V-ATPase subunit F provides structural similarities and diversities to subunit F of the related A_1A_O ATP synthases and thereby shows the structural basis toward a better understanding of the static and mechanistic properties of this subunit inside the V_1 and V_1V_O ATPase.

Acknowledgements

Sandip Basak, Shovanlal Gayen and Youg R. Thaker are grateful to the Nanyang Technological University for awarding research scholarship. This research was supported by A*STAR BMRC (09/1/22/19/609).

References

[1] S. Saroussi, N. Nelson, Vacuolar H^+-ATPase — an enzyme for all seasons, Pfluegers Arch.–Eur. J. Physiol. 457 (2009) 581–587.
[2] K.W. Beyenbach, H. Wieczorek, The V-type H^+ ATPase: molecular structure and function, physiological roles and regulation, J. Exp. Biol. 209 (2006) 577–589.
[3] V. Marshansky, The V-ATPase a2-subunit as a putative endosomal pH-sensor, Biochem. Soc. Trans. 35 (2007) 1092–1099.
[4] J.S. Lolkema, Y. Chaban, E.J. Boekema, Subunit composition, structure, and distribution of bacterial V-Type ATPase, J. Bioenerg. Biomembr. 35 (2003) 323–336.
[5] C. Kluge, J. Lahr, M. Hanitzsch, S. Bolte, D. Golldack, K.J. Dietz, New insight into the structure and regulation of the plant vacuolar H^+-ATPase, J. Bioenerg. Biomembr. 35 (2003) 377–388.
[6] G. Grüber, V. Marshanski, New insights into structure–function relationships between archeal ATP synthase (A_1A_O) and vacuolar type ATPase (V_1V_O), Bioessays 30 (2008) 1096–1099.
[7] T. Nishi, M. Forgac, The vacuolar (H+)-ATPases-nature's most versatile proton pumps, Nat. Mol. Cell. Biol. 30 (2002) 94–103.
[8] O. Drory, F. Frolow, N. Nelson, Crystal structure of yeast V-ATPase subunit C reveals its stator function, EMBO Rep. 5 (2004) 1148–1152.
[9] S. Rishikesan, S. Gayen, R.Y. Thaker, S. Vivekanandan, M.S.S. Manimekalai, Y.H. Yau, S. Geifman Shochat, G. Grüber, Assembly of subunit *d* (Vma6p) and G (Vma10p) and the NMR solution structure of subunit G ($G_{1–59}$) of the *Saccharomyces cerevisiae* V_1V_O ATPase, Biochim. Biophys. Acta - Bioenergetics 1787 (2009) 242–251.
[10] S. Rishikesan, M.S.S. Manimekalai, G. Grüber, The NMR solution structure of subunit G (G_{61-101}) of the eukaryotic V_1V_O ATPase *Saccharomyces cerevisiae*, Biochim. Biophys. Acta - Biomembranes 1788 (2010) 1961–1968.
[11] M. Sagermann, T.H. Stevens, B.W. Matthews, Crystal structure of the regulatory subunit H of the V-type ATPase of *Saccharomyces cerevisiae*, Proc. Natl. Acad. Sci. U. S. A. 98 (2001) 7134–7139.
[12] M. Radermacher, T. Ruiz, H. Wieczorek, G. Grüber, The structure of the V_1-ATPase determined by three-dimensional electron microscopy of single particles, J. Struct. Biol. 135 (2001) 26–37.
[13] G. Grüber, M. Radermacher, T. Ruiz, J. Godovac-Zimmermann, B. Canas, D. Kleine-Kohlbrecher, M. Huss, W.R. Harvey, H. Wieczorek, Three-dimensional structure and subunit topology of the V_1 ATPase from *Manduca sexta* midgut, Biochemistry 39 (2000) 8609–8616.
[14] Ü. Coskun, V.F. Rizzo, M.H.J. Koch, G. Grüber, Ligand-dependent structural changes in the V_1 ATPase from *Manduca sexta*, J. Bioenerg. Biomembr. 36 (2004) 249–256.
[15] K.J. Parra, K.L. Keenan, P.M. Kane, The H subunit (Vma13p) of the yeast V-ATPase inhibits the ATPase activity of cytosolic V_1 complexes, J. Biol. Chem. 275 (2000) 21761–21767.
[16] K.C. Jefferies, M. Forgac, Subunit H of the V-ATPase inhibits ATP hydrolysis by the free V_1 domain by interaction with the rotary subunit F, J. Biol. Chem. 283 (2007) 4512–4519.
[17] G. Grüber, J. Godovac-Zimmermann, T.A. Link, Ü. Coskun, V.F. Rizzo, C. Betz, S.M. Bailer, Expression, purification, and characterization of subunit E, an essential subunit of the vacuolar ATPase, Biochem. Biophys. Res. Commun. 298 (2002) 383–391.
[18] U. Laemmli, Cleavage of structural proteins during the assembly of the head of bacteriophage T4, Nature 227 (1970) 680–685.
[19] P. Manavalan, W.C. Johnson, Variable selection method improves the prediction of protein secondary structure from circular dichroism spectra, Anal. Biochem. 167 (1987) 76–85.
[20] N. Sreerama, R.W. Woody, A self-consistent method for the analysis of protein secondary structure from circular dichroism, Anal. Biochem. 209 (1993) 32–44.
[21] S.W. Provencher, A constrained regularization method for inverting data represented by linear algebraic or integral equations, Comput. Phys. Commun. 27 (1982) 213–227.
[22] M.A. Andrade, P. Chacon, J.J. Merelo, F. Moran, Evaluation of secondary structure of proteins from UV circular dichroism spectra using an unsupervised learning neural network, Protein Eng. Des. Sel. 6 (1993) 383–390.
[23] G. Deléage, C. Geourjon, An interactive graphic program for calculating the secondary structure content of proteins from circular dichroism spectrum, Comput. Appl. Biosci. 9 (1993) 197–199.
[24] G. Bohm, R. Muhr, R. Jaenicke, Quantitative analysis of protein far UV circular dichroism spectra by neural networks, Protein Eng. Des. Sel. 5 (1992) 191–195.
[25] L. Whitmore, B.A. Wallace, DICHROWEB, an online server for protein secondary structure analyses from circular dichroism spectroscopy data, Nucleic Acids Res. 32 (2004) W668–W763.
[26] C. Boulin, R. Kempf, M.H.J. Koch, S.M. McLaughlin, Data appraisal, evaluation and display for synchrotron radiation experiments: hardware and software, Nucl. Instrum. Methods Phys. Res., Sect. A 249 (1986) 399–407.
[27] M. Roessle, R. Klaering, U. Ristau, B. Robrahn, D. Jahn, T. Gehrmann, P.V. Konarev, A. Round, S. Fiedler, S. Hermes, D.I. Svergun, Upgrade of the small angle X-ray scattering beamline X33 at the EMBL Hamburg, J. Appl. Crystallogr. 40 (2007) 190–194.
[28] A.R. Round, D. Franke, S. Moritz, R. Huchler, M. Fritsche, D. Malthan, R. Klaering, D.I. Svergun, M. Roessle, Automated sample-changing robot for solution scattering experiments at the EMBL Hamburg SAXS station X33, J. Appl. Cryst. 41 (2008) 913–917.
[29] D. Svergun, A direct indirect method of small-angle scattering data treatment, J. Appl. Crystallogr. 26 (1993) 258–267.
[30] A. Guiner, G. Fournet, Small Angle Scattering of X-ray, Wiley, New York, 1955.
[31] D.I. Svergun, M.V. Petoukhov, M.H.J. Koch, Determination of domain structure of proteins from X-ray solution scattering, Biophys. J. 80 (2001) 2946–2953.
[32] D.I. Svergun, Restoring low resolution structure of biological macromolecules from solution scattering using simulated annealing, Biophys. J. 76 (1999) 2879–2886.
[33] D.I. Svergun, A. Bećirević, H. Schrempf, M.H.J. Koch, G. Grüber, Solution structure and conformational changes of the streptomyces chitin binding protein (CHB1), Biochemistry 39 (2000) 10677–10683.
[34] V.V. Volkov, D.I. Svergun, Uniqueness of *ab initio* shape determination in small angle scattering, J. Appl. Cryst. 36 (2003) 860–864.

[35] T. Goddard, D. Kneller, SPARKY 3, University of California, San Francisco, CA, 1997.
[36] K. Wüthrich, NMR of Proteins and Nucleic Acids, Wiley, Interscience, New York, 1986.
[37] G. Cornilescu, F. Delaglio, A. Bax, Protein backbone angle restraints from searching a database for chemical shift and sequence homology, J. Biomol. NMR 13 (1999) 289–302.
[38] P. Güntert, C. Mumenthaler, K. Wüthrich, Torsion angle dynamics for NMR structure calculation with the new program D, J. Mol. Biol. 273 (1997) 283–298.
[39] H.D.T. Mertens, D.I. Svergun, Structural characterization of proteins and complexes using small-angle X-ray solution scattering, J. Struct. Biol. 172 (2010) 128–141.
[40] D.I. Svergun, S. Konrad, M. Huss, M.H.J. Koch, H. Wieczorek, K. Altendorf, V.V. Volkov, G. Grüber, Quaternary structure of V_1 and F_1 ATPase: significance of structural homologies and diversities, Biochemistry 37 (1998) 17659–17663.
[41] I. Schäfer, M. Rössle, G. Biuković, V. Müller, G. Grüber, Structural and functional analysis of the coupling subunit F in solution and topological arrangement of the stalk domains of the methanogenic A_1A_O ATPsynthase, J. Bioenerg. Biomembr. 38 (2006) 83–92.
[42] A. Armbrüster, D.I. Svergun, Ü. Coskun, S. Juliano, S.M. Bailer, G. Grüber, Structural analysis of the stalk subunit Vma5p of the yeast V-ATPase in solution, FEBS Lett. 570 (2004) 119–125.
[43] A.C. Hausrath, G. Grüber, B.W. Matthews, R.A. Capaldi, Structural features of the γ subunit of the *Escherichia coli* F_1 ATPase revealed by a 4.4 Å resolution map obtained by X-ray crystallography, Proc. Natl. Acad. Sci. U. S. A. 96 (1999) 13697–13702.
[44] G. Vaaje-Kolstad, D.R. Houston, A.H.K. Riemen, V.G.H. Eijsink, D.M.F. van Aalten, Crystal structure and binding properties of the *Serratia marcescens* chitin-binding protein CBP21, J. Biol. Chem. 280 (2005) 11313–11319.
[45] S. Gayen, S. Vivekanandan, G. Biuković, G. Grüber, H.S. Yoon, Backbone ^{1}H, ^{13}C, and ^{15}N resonance assignments of subunit F of the A_1A_O ATP synthase from *Methanosarcina mazei* Gö1, Biomol. NMR Assign. 1 (2007) 23–25.
[46] S. Gayen, S. Vivekanandan, G. Biuković, G. Grüber, H.S. Yoon, The NMR solution structure of subunit F of the methanogenic A_1A_O ATP synthase and its interaction with the nucleotide-binding subunit B, Biochemistry 46 (2007) 11684–11694.
[47] H. Makyio, R. Iino, C. Ikeda, H. Imamura, M. Tamakoshi, M. Iwata, D. Stock, R.A. Bernal, E.P. Carpenter, M. Yoshida, K. Yokoyama, S. Iwata, Structure of a central stalk subunit F of prokaryotic V-type ATPase/synthase from *Thermus thermophilus*, EMBO J. 24 (2005) 3974–3983.
[48] D. Raghunathan, S. Gayen, G. Grüber, C. Verma, Crosstalk along the stalk: dynamics of the interaction of subunits B and F in the A_1A_O ATP synthase of *Methanosarcina mazei* Gö1, Biochemistry 49 (2010) 4181–4190.
[49] Y.L. Chaban, S. Juliano, E.J. Boekema, G. Grüber, Interaction between subunit C (Vma5p) of the yeast vacuolar ATPase and the stalk of the C-depleted V_1 ATPase from *Manduca sexta* midgut, Biochim. Biophys. Acta – Bioenergetics 1708 (2005) 196–200.
[50] T. Xu, E. Vasilyeva, M. Forgac, Subunit interactions in the clathrin-coated vesicle vauolar (H^+)-ATPase complex, J. Biol. Chem. 274 (1999) 28909–28915.
[51] T.E. Creighton, Disulfide bond formation in proteins, Methods Enzymol. 107 (1984) 305–329.
[52] R. Gräf, W.R. Harvey, H. Wieczorek, Cloning, sequencing and expression of cDNA encoding an insect V-ATPase subunit E, Biochim. Biophys. Acta – Biomembranes 1190 (1994) 193–196.
[53] R. Gräf, A. Lepier, W.R. Harvey, H. Wieczorek, A novel 14-kDa V-ATPase subunit in the tobacco hornworm midgut, J. Biol. Chem. 269 (1994) 3767–3774.
[54] M.V. Berjanskii, S. Neal, D.S. Wishart, PREDITOR: a web server for predicting protein torsion angle restraints, Nucleic Acids Res. 34 (2006) 63–69.
[55] W.L. DeLano, The pyMol Molecular Graphics System, DeLano Scientific, San Carlos, CA, 2001.